Accurate Density Functional Calculations of Core Electron Binding Energies on Hydrogen-Bonded Systems

Philippe Aplincourt,[†] Christophe Bureau,*[,†] Jean-Luc Anthoine,[‡] and Delano P. Chong[†,§]

CEA-Saclay, DSM-DRECAM-SPCSI, bât 466, F-91191 Gif-sur-Yvette Cedex, France, and Laboratoire d'Informatique de l'Université de Franche-Comté, IUT de Belfort-Montbéliard, B.P. 527, Rue Engel Gros, F-90016 Belfort Cedex, France

Received: January 4, 2001; In Final Form: May 11, 2001

We present a quantum chemical investigation of core−electron binding energies (CEBEs) for small hydrogen-bonded clusters involving water, carboxylic acids, and formamide. Our DFT ΔE_{KS} method well reproduces scarce experimental CEBEs available in the literature, especially the recent ones on gas phase water clusters. This shows that hydrogen bonds are actually detectable using XPS, even though it is a core level probing technique. This may be of major interest for hydrogen bonding detection in very thin layers, for which few methods may have the required sensitivity. A correlation is further established between hydrogen bond lengths in the cluster and binding energy shifts, as a function of cluster size. Unlike what is concluded for rare gas clusters, these shifts may be uniquely connected to intramolecular geometrical rearrangements, rather than collective spherical-type relaxation effects. This may also lead to the possibility of a direct measure of mean bond lengths in associated materials (solid, liquid, or gas) using XPS.

1. Introduction

X-ray photoelectron spectroscopy is among the very powerful techniques to gain information on the chemical composition and bonding for molecules, surfaces, and interfaces.[1] Core−electron binding energies (CEBEs) constitute the key spectral information obtained by this technique, as they are related to the physicochemical environment a nucleus feels in a molecule.[2] Early in the history of XPS, it was recognized that the CEBE of an atom should be related to the effective charge on that atom.[3,4] This effective charge could in turn be correlated with intuitive concepts such as the difference between the electronegativity of bonded atoms.[5] From these empirical correlations emerged a rule-of-thumb stating that the CEBE of an atom is raised when it is in a more electronegative surrounding, and that it is lowered when experiencing the effects of a more electropositive environment.[1] Despite the invaluable practical usefulness of this simple rule, it is sometimes difficult to relate precisely the various CEBEs with the underlying molecular structures. The difficulty is particularly important when the CEBEs differ by a few electronvolts or fraction of an electronvolts because the typical resolution of XPS experiments is in general on the order of 0.2−0.5 eV. It may be as low as 0.05 eV when the irradiation is performed with synchrotron radiation. In these cases, theoretical calculations have proven quite useful or even indispensable to a correct interpretation.[6−8]

Recently, one of us proposed a series of methods making use of density functional (DFT) calculations,[9,10] enabling the very accurate calculation of CEBEs in molecular systems. The uGTS method is based on a generalization of Slater's transition-state (TS) approach[11,12] and has now been tested on more than 200 molecules. It deliver predicted CEBEs in excellent agreement with experiment, with an average absolute deviation from experiment (aad) of only 0.20 eV,[13,14] i.e., equivalent to the best available resolution on a spectrometer. Even better results were obtained using the so-called "Delta-*E*" (ΔE) approach, in which the explicit calculation is carried out on both the neutral parent and the core-ionized species.[10,15]

The interest of such accurate methods is that they may be used as probes, helping one to deduce molecular structures with a relatively high degree of precision and little ambiguity. This strategy has been used with success, e.g., to assess the structural stability of (γ-aminopropyl)triethoxysilane (γ-APS: $H_2N-CH_2-CH_2-CH_2-Si(OCH_2CH_3)_3$) upon adsorption onto a silicon surface.[16] The elucidation power of the method, in terms of molecular structures, is also facilitated by the fact that calculations can be made on rather poor geometries, such as those obtained at the semiempirical level.[17]

In a few instances, however, we have noticed that taking correct molecular structures into account was insufficient to reach a theory vs experiment agreement compatible with the resolution of the method.[13,16] In these cases, it was proposed that the discrepancies could well be attributable to intermolecular effects. An example is given with the γ-APS molecule. Exposure of this compound to atmosphere (H_2O/CO_2) leads to the formation of an ionic pair between ammonium ($-NH_3^+$) groups and hydrogen carbonate ions (HCO_3^-). We have shown that the N(1s) line of the ammonium group is downshifted by about 2 eV when one actually makes the calculation on the ion pair (402.18 eV) instead of the sole ammonium (404.09 eV). This same line is still downshifted by about 0.3 0.6 eV (401.85 401.58 eV) when one also explicitly includes a first layer of water molecules in the model, meant to reproduce the local "solvating" environment.[16] This suggests that with the help of very accurate calculations, even intermolecular effects may be detectable using XPS.

This proposal may seem surprising at first, since most intermolecular energies are 2 or 3 orders of magnitude weaker

* Corresponding author. E-mail: christophe.bureau@cea.fr.
† CEA-Saclay.
‡ Laboratoire d'Informatique de l'Université de Franche-Comté.
§ On leave from: Department of Chemistry, University of British Columbia, 2036 Main Mall, Vancouver, BC V6T 1Z1, Canada.

10.1021/jp0100194 CCC: $20.00
Published on Web 07/11/2001

than the ones typically involved in XPS experiments, which is essentially a technique probing core levels. One should keep in mind, however, that XPS probes densities rather than energies, in a way pretty similar to nuclear magnetic resonance (NMR). Relaxation, correlation effects, and electrostatic influences from surrounding atoms or molecules monitor the sign and magnitude of chemical shifts from one atom of a given type to another (one may note that even though the physical process are different, NMR and XPS chemical shifts of a given atom are nicely correlated on most systems).[18]

In the present paper, we bring arguments to the above proposal, focusing essentially on the effect of hydrogen bonds on CEBEs. Hydrogen bonds are thought to be decisively involved in the structural arrangement of unbound rings in catenanes and rotaxanes.[19] These macromolecules are of great interest in the design of surfaces functionalized with conformational triggers. While their intermolecular hydrogen bonds are easily detectable both in solution and in the solid state, thus characterizing their conformational state, they are difficult to assess when the molecules are deposited on a surface at the monolayer scale: infrared reflection absorption spectroscopy (IRRAS) nor NMR are sensitive enough. XPS, as a traditional tool in surface analysis, may then turn out to be the only possibility to prove conformational triggering, provided that the evidencing of hydrogen bonds with XPS may be achieved.

Our first task, contained in the results of the present paper, is to demonstrate on suitable benchmark systems, that hydrogen bonds are detectable with core XPS. The issue of more complex molecules is addressed in another paper. Toward this aim, we have performed highly accurate XPS calculations using the ΔE approach on three kinds of systems structured thanks to a hydrogen bond network: (i) clusters of water molecules $(H_2O)_n$ in the gas phase; (ii) formic and acetic acid dimers, in which the carboxylic groups act as both hydrogen bond donors and acceptors; (iii) formamide oligomers, in which the carbonyl group acts as a hydrogen bond acceptor while the vicinal amine group acts as a hydrogen bond donor.

Recent accurate experimental values are available for case i.[20] This enables a direct comparison with our theoretical models and allows an evaluation of the quality of the predictions. We are not aware of experimental data available for cases ii and iii. However, these examples have been chosen in order to gain insight into possible additive effects when hydrogen bond donation combines with hydrogen bond acceptance on a single functional group. This latter concern is also meant to examine whether the present, dedicated, orders of magnitude may be transferable to similar functional groups in a different molecule, thus providing a systematic evaluation for experimental interpretation (and allowing, to some extent, a bypass of systematic calculations).

2. Computational Details

The DFT calculations have been done with the deMon code[21] on a cluster of Pentium II under Linux (Debian). The set of auxiliary basis functions is (4,4;4,4) for C, N and O and (3,1;3,1) for H.[22] The orbital basis sets are Dunning's cc-pVTZ on C, N, O and H.[23] As previously,[24] scaled-pVTZ basis sets have also been used on the partially ionized atomic centers in order to better describe the core−hole. The results obtained with all these basis sets are compared. Only s-, p- and (six components) d-type functions were used. The numerical integration for the fit of the exchange and correlation potentials into the auxiliary basis set is performed using a grid having 32 radial points × 194 angular points per atom. The functionals are Perdew and Wang's 1986[25] for the exchange term and Perdew and Wang's 1991[26] for the correlation term.

To compare the calculated CEBEs with experiment, we need an evaluation of relativistic effects (which we do not take into account explicitly in the quantum mechanical treatment). A crude estimate of relativistic corrections C_{rel} can be made by adding to the theoretical values the quantity:[24]

$$C_{rel} = K I_{nr}^{N}$$

where $K = 2.198 \times 10^{-7}$ and $N = 2.178$, when both I_{nr} and C_{rel} are in electronvolts. In this expression, I_{nr} represents the nonrelativistic CEBE. In what follows, all CEBE values are referenced to the vacuum level, unless otherwise mentioned.

Geometries of the various water cluster $(H_2O)_n$ ($n = 2-6$) have been previously optimized at the MP2/aug-cc-pVDZ level.[27] In their study, Xantheas et al. have shown that this method, used with this basis set, yields accurate results as far as the structure of the monomer and dimer of water molecule are concerned.[28] Therefore, this method appears to be adequate to describe the structure of larger clusters. In the cases of formic and acetic acid monomers and dimers as well as formamide, we got the experimental geometries from convenient compilations.[29] Formamide−water complexes have been optimized at the MP2/aug-cc-pVDZ level using the Gaussian98 program.[30]

3. Results and Discussion

Figures 1, 4, 5, and 6 display the geometries of all the compounds considered in our study. Tables 1−4 gather the computed CEBEs, whereas additional results are reported in Figures 2 and 3.

Water Clusters. In a recent paper, Björnehom et al. presented a photoemission study of water clusters with a value of n up to 250.[20] These authors have also measured that the O(1s) binding energy decreases as a function of cluster size. The binding energy shift found between the molecule and the smallest cluster ($n = 20$) was equal to 1.1 eV, and even reached 1.3 eV for a very high degree of condensation.

Figure 1 displays all the water clusters considered in this study. For a given value of n, numerous minima may exist on the potential energy surface. For the water hexamer, for example, Kryachko located 15 different local minima very close to the global minimum.[31] In our work, we considered, for each cluster, the most stable structures only, for $n = 1-6$.

Table 1 presents the O(1s) CEBEs and binding energy shifts of the clusters that we studied. The O(1s) binding energy shift of clusters containing nonequivalent oxygen atoms was assumed to be equal to the average of the binding energy shift of each oxygen atom within the cluster. In Figure 2, we plotted the variation of this shift as a function of cluster size. One may first notice that the predicted shifts have the correct sign, i.e., the O(1s) CEBEs decrease as a function of cluster size.

Moreover, we find that the larger the size of the cluster, the larger the shift, with an apparent asymptote toward the experimental shift measured for small clusters, i.e., 1.1 eV. One shall note that the point associated with the dimer, the only noncyclic molecule, is slightly off the theoretical curve. This may be due to the fact that, in the dimer, the two water molecules have distinct roles, one being the proton donor whereas the other one is the proton acceptor, while all water molecules play both roles at the same time in higher (cyclic) clusters.

On the basis of previous investigations on argon clusters,[32,33] Björnehom et al. conclude that the lowering of the binding

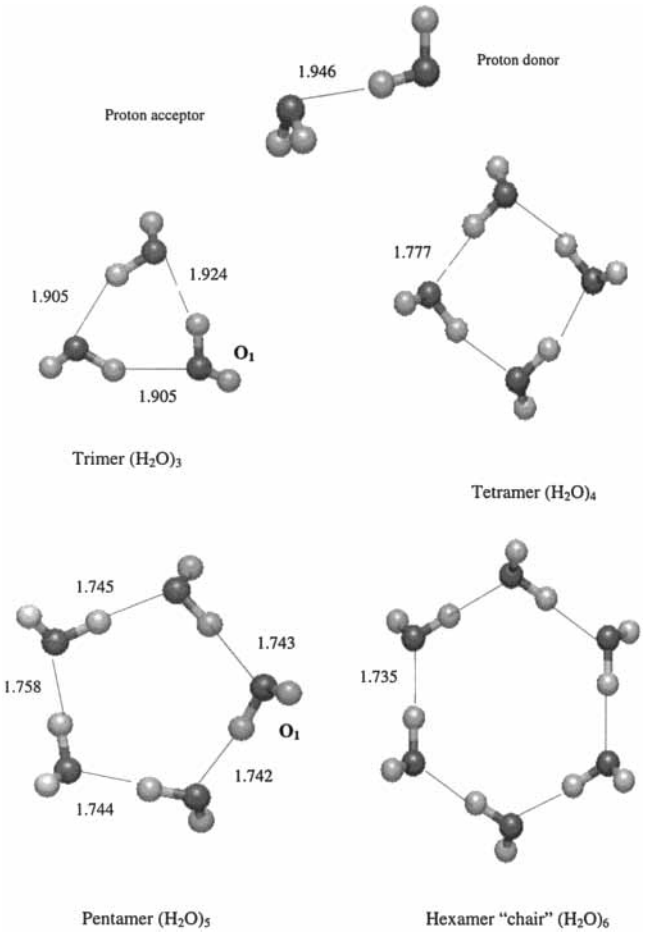

Figure 1. Geometries of the water clusters $(H_2O)_n$ ($n = 2-6$) studied. In the $n = 3$ and $n = 5$ $(H_2O)_n$ clusters, the oxygen atoms have been numbered clockwise starting from the O_1 atom. Distances are given in angströms.

TABLE 1: O(1s) CEBE (eV) of the Water Molecule and the Water Clusters Considered $(H_2O)_n$ ($n = 2-6$)

cluster	atom	CEBE	shift O···H	average shift
$n = 1$	O	539.95		
$n = 2$	acceptor	540.58	+0.63	−0.63
	donor	538.69	−1.26	
$n = 3$	O_1	539.29	−0.66	−0.62
	O_2	539.33	−0.62	
	O_3	539.37	−0.58	
$n = 4$	O	539.13[a]	−0.82	−0.82
$n = 5$	O_1	539.02	−0.93	−0.93
	O_2	539.02	−0.93	
	O_3	539.07	−0.88	
	O_4	539.00	−0.95	
	O_5	539.01	−0.94	
$n = 6$	O	538.97[a]	−0.98	−0.91
chair	O	539.12[a]	−0.83	
prism	O	539.05[a]	−0.90	
cage	O	539.01[a]	−0.94	
book				

[a] This value refers to the average of computed O(1s) CEBEs over all the oxygen atoms in the given structure.

energy as a function of the cluster size is due to polarization screening in the final state, which increases with cluster size.[20] There are two types of atoms in argon clusters: surface and bulk. Atoms surrounding the core ionized atom are polarized, and this polarization decreases rapidly with increasing distance from the ionized atom. Therefore, nearest neighbors are the most important ones for the screening, and an atom with a large

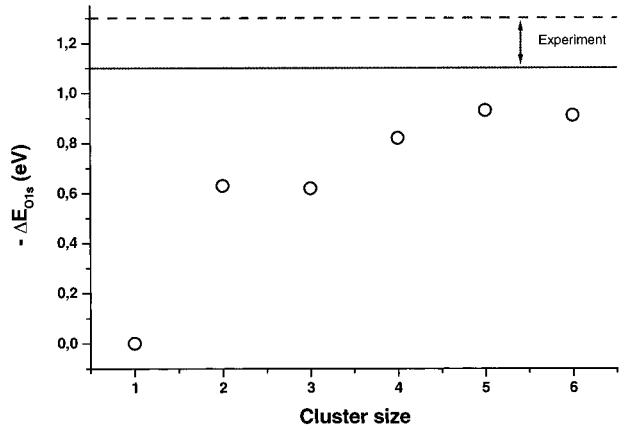

Figure 2. Evolution of the binding shift eV) as a function of the cluster size. The continuous line (−1.1 eV) represents the experimental binding energy shift between molecule and small clusters (about $n = 20$).[20] The dotted line (−1.3 eV) represents the binding energy shift measured for a very high degree of condensation.[20]

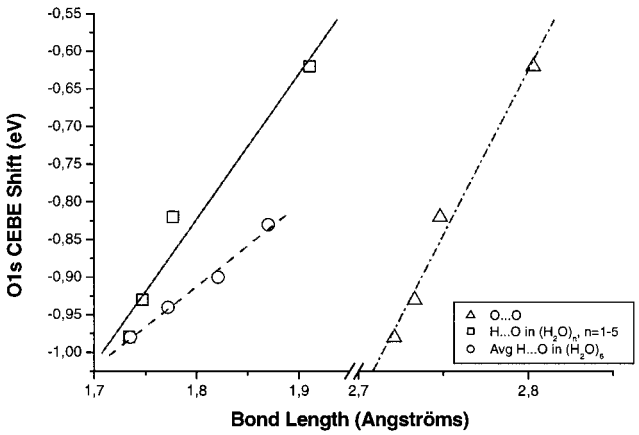

Figure 3. O(1s) binding energy shifts (eV) as a function of O−O and O...H distances (Å) for water clusters (Figures 1 and 4). The lines represent tentative fits and only constitute a guide to the eye.

number of nearest neighbors, as in the interior of the cluster, yield a large shift. On the basis of these arguments, Björnehom et al. concluded that the larger the cluster size, the larger the fraction of atoms in the bulk and the lower the corresponding binding energy.

In our investigation of small water clusters, the notion of surface and bulk disappears. In addition, in all clusters, excepted in the dimer, each water molecule has the same number of neighbors, i.e., two. Therefore, we felt that the lowering of the O(1s) binding energies should be accounted for on different grounds.

In these clusters, water molecules are hydrogen bonded whereas in argon clusters, there are van der Waals interactions. The electrostatic origin of hydrogen bonding is actually favored. Buckingham et al.[34] have shown that the electrostatic interaction, computed via distributed multipole moments, coupled with a simple hard-sphere atom−atom repulsion, gives a good account of the structures of numerous hydrogen-bonded systems. Furthermore, in a previous theoretical study on small water clusters, Xantheas et al. observed structural trends associated with the cluster size.[28] In particular, the separation between neighboring oxygen atoms decreases exponentially with increasing cluster size.

Figure 3 displays the variation of the O−O and O...H distances as a function of the binding energy shift. One can notice a clear correlation between both O−O and O...H

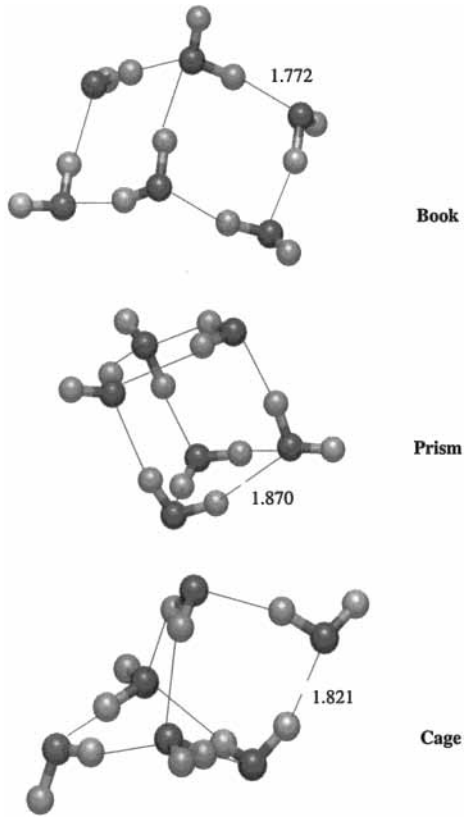

Figure 4. Geometries of the three additional conformers of water hexamer $(H_2O)_6$ studied in this work. From top to bottom, the book, prism, and cage conformers. Distances are given in angströms.

TABLE 2: Average Hydrogen Bond Lengths (Å) and Average Binding Energy Shifts (eV) of the Four Conformers of Water Hexamer Envisaged in This Study

conformers	average H bond lengths	average binding energy shifts
chair	1.735	−0.98
book	1.772	−0.94
cage	1.821	−0.90
prism	1.870	−0.83

distances, and the corresponding O(1s) binding energy shift. One may therefore propose that the O(1s) binding energy shifts in water clusters are mainly caused by geometrical rearrangements, via the interplay of electrostatic effects.

This proposal may be further checked by examining whether the same trend is observed for water clusters with the same number of molecules, but a different relative arrangement. Water hexamer seems appropriate to verify this hypothesis, as this cluster presents many conformers. MP2(full)/aug-cc-pVDZ calculations show that the prism conformer is the global minimum.[31] Secondary minima have been evidenced, and four different conformers of $(H_2O)_6$ were considered herein: chair, book, cage, and prism (Figures 1 and 4). Their structures have been optimized at the MP2(full)/aug-cc-pVDZ level.[27] Both the average bond distances per conformer and the average O(1s) binding energy shifts are gathered in Table 2.

The highest average O(1s) shift is associated with the chair conformer (−0.98 eV), in which the hydrogen bond distances are smallest (1.735 Å). Conversely, the smallest average shift is obtained with the prism conformer (−0.83 eV), in which hydrogen bond distances are highest (1.870 Å). As in the case of water cluster $(H_2O)_n$ conformer-averaged O(1s) CEBEs as a function of cluster size, a linear correlation is found between hydrogen bond distances and O(1s) CEBEs (see Figure 3).

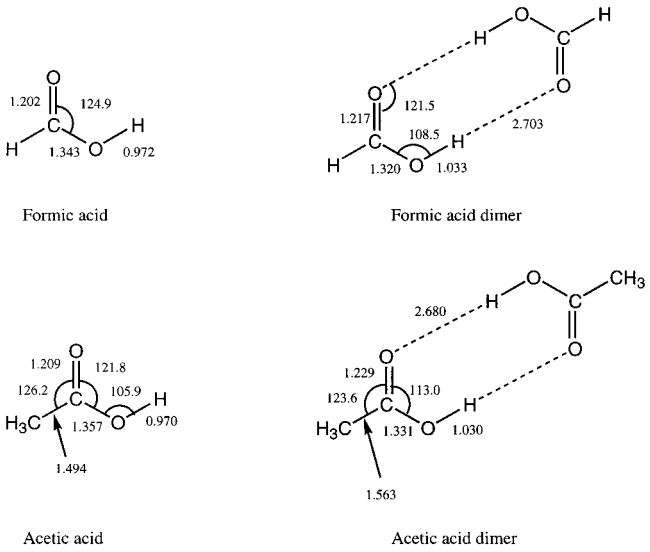

Figure 5. Geometries of formic and acetic acid dimers. The corresponding monomers are also pictured. Distances are given in angströms and angles in degrees.

This suggests that at least a practical relationship exists between the average hydrogen bond lengths within the cluster and the calculated binding energy shifts. Our present estimates indicate that this is true to a large extent whatever the size of the cluster and the relative arrangement of the water molecules within the clusters. Therefore, CEBEs may constitute an interesting way to obtain the average length of hydrogen bonds for a given cluster.

The following examples deal with structures on which no experimental data are available, to our knowledge. Taking for granted that our calculation method is probably well suited to determine CEBEs on hydrogen-bonded systems, we now scan various systems involving hydrogen bonds. We have checked whether O(1s) shifts as large as those obtained with water clusters may be expected on other systems and constitute a general trend.

Formic and Acetic Acid. The formic acid dimer is the smallest carboxylic acid dimer. It has been widely investigated experimentally[35−38] as well as theoretically[39−48] because of the presence of two strong hydrogen bonds between the two monomers. This dimer is indeed a simple system that involves double proton transfer. This phenomenon is part of many chemical and biochemical reactions that are of interest as proton relay systems in enzymes. Several theoretical studies have detailed this double transfer.[43−48] The results suggest a synchronous transfer as well as a very efficient tunneling effect, with a tunneling path very different from the minimum energy path.[45]

Figure 5 points out the experimental geometries of the formic acid dimer, the acetic acid dimer, and the corresponding monomers. The formation of each dimer goes along with a decrease of the C−O bond length and an increase of the C═O bond length. The variations of length for these two bonds are approximately of the same extent.

Table 3 gathers the O(1s) CEBEs of the aforementioned dimers and monomers. We compared the data obtained on the monomers with experiment. Our results are in good agreement with experiment,[10,49] which confirms the accuracy of the theoretical ΔE_{KS} method. For both acids, the most important discrepancies are obtained in the case of the oxygen atom of the hydroxyl group. For this atom, the average deviation from experiment is found to be 0.20 eV, whereas it is found to be 0.07 eV for the oxygen atom of the carbonyl group. In addition,

TABLE 3: O(1s) CEBE (eV) for the Monomers and Dimers of the Formic and Acetic Acids[a]

	monomer			
	experiment	DFT	dimer DFT	shift DFT
HC*O*OH	538.97	538.90	539.05	+0.15
HCO*O*H	540.63	540.88	540.07	−0.81
$CH_3C*O*OH$	538.33	538.27	538.28	+0.01
$CH_3CO*O*H$	540.12	540.27	539.57	−0.70

[a] In the last column, we report the binding energy shift due to the formation of dimers

our calculations exhibit binding energy shift between the monomer and the dimer. First of all, we point out that the difference between CEBEs of both oxygen atoms decrease from the monomer (1.98 eV for HCOOH; 2.00 eV for CH_3COOH) to the dimer (1.02 eV for HCOOH; 1.29 eV for CH_3COOH). If we refer to the double proton-transfer reaction in the formic acid dimer (FAD), we can note that this trend is correct. During this reaction, there is a synchronous double proton transfer, as pictured in Scheme 1:

The structure of the transition state associated with this reaction (FADTS) is of D_{2h} symmetry. It possesses four equivalent O...H bonds (see Scheme 1). Therefore, the CEBEs of all four oxygens are the same. As one moves onto the transition state on the potential energy surface toward the formic acid dimer, the distance between the two monomers increases. The oxygen atoms of a given monomer become nonequivalent and CEBEs of these two atoms will be different. The larger the distance between the two monomers, the larger the energy difference between both oxygen atoms. Therefore, it is natural to observe a more important difference in the dimer than in the monomer because the structure of the latter can be viewed as the same one encountered in a dimer with an infinite distance between the two moieties.

For both acids, we can see in Table 3 that the shift associated with the oxygen atom of the hydroxyl group (−0.81 eV and −0.70 eV for the formic and acetic acids respectively) is more important than the one computed for the oxygen atom of the carbonyl group (+0.15 and +0.01 eV, respectively). These results correctly reproduce the effect of the two hydrogen bonds since the geometrical structure, and therefore the electronic density, change more around the oxygen atom of the hydroxyl group with the formation of the dimer.

Moreover, Qian et al.[40] calculated the dipole-derivative derived charges at the HF/6-311++G** and showed that the changes in the atomic charges are largest for the oxygen atom of the hydroxyl group than for the oxygen atom of the carbonyl group.

Formamide. Formamide is the simplest compound that contains the essential features of the peptide linkage. Several investigations have been devoted to the study of formamide with water molecules because these complexes can be used as simple models for the hydration of peptides or proteins.[50−54] Studies have been reported on the stability and the structure of the complex with water[50−52] or on proton-transfer reaction.[53,54] Here, we consider two formamide−water complexes. The formamide is in its keto form in one complex and in its enol form (formamidic acid) in the other one (see Figure 6). They are bidentate systems where water participates in two hydrogen bonds, one as a donor and one as an acceptor. Table 4 displays binding energies of all the heavy atoms of the two forms of the formamide molecule and the two formamide−water complexes.

First, binding energies computed for the keto and enol forms have been compared with results found in the case of formamide and formamidic acid. The observed binding energy shifts vary from one atom to the other. In the keto form, we observe an increase of the O(1s) binding energy (+0.15 eV) because the O atom possesses a proton-acceptor character. Conversely, the N atom is a proton-donor and we therefore notice a lowering of the N(1s) binding energy (−0.24 eV). The C(1s) binding energy varies only very slightly from the formamide to the complex because the carbon atom is not hydrogen-bonded. For the enol form, the same trend is observed if we refer to the formamidic acid. In this form, the O atom is proton-donor and the a decreasing of the O(1s) CEBE is observed from the acid to the complex (−0.53 eV). The N atom is proton-acceptor and the binding energy increases very slightly from the acid to the complex (+0.04 eV). As for the keto form, the C(1s) binding energy has quite the same value in the acid and in the complex (−0.05 eV).

Second, binding energies calculated for the O atom of the water moiety in each complex have also been compared with the value obtained for the sole water molecule (539.95 eV). In both complexes, the O atom has the two proton-donor and proton-acceptor roles. Therefore, as for the water clusters, the O(1s) line is downshifted in the keto form (−1.06 eV) as well as in the enol form (−0.79 eV).

Core electron binding energies of C, N, and O atoms computed for the two formamide complexes vary to different extents from the keto to the enol form. For the carbon atom, the calculated shift is only due to geometry changes in the formamide moiety. The geometric and electronic environments close to this atom are not much modified from the keto form to the enol one. Therefore, the binding energy shift is not important (−0.29 eV). The case of nitrogen and oxygen atoms is different because the geometry of the molecule around these two atoms is more modified than in the case of the carbon atom, but there is especially a large modification of the length of hydrogen bonds. For the oxygen and nitrogen atoms of the formamide moiety, we respectively notice a large increase and a large decrease of computed CEBEs. We have shown previously for water clusters that CEBEs increase with a decrease of the hydrogen bond length. In the case of formamide−water complexes, the hydrogen bond involving the oxygen atom in the keto form shortens and forms an O−H covalent bond in the enol form. Therefore, this large shortening is accompanied by a large increase of CEBE (+1.85 eV). Conversely, the initial N−H covalent bond in the keto form lengthens to a large extent to yield a hydrogen bond N...H in the enol form. CEBE of the N atom is consequently lower in the enol form (−1.48 eV).

Variation of O(1s) CEBE for the oxygen atom of the water moiety have retained more attention. At first sight, the negative binding energy shift is larger in the keto form by 0.27 eV, whereas the overall hydrogen bond length is shorter in the enol form (1.883 Å vs 1.963 Å). This result is a priori in contradiction with the one found for the water clusters. However, two factors allow us to explain this discrepancy. First, we have seen, in Table 1, that the proton-donor character of the oxygen atom yields to a much more important binding energy shift than the proton-acceptor character (by a factor 2 in the case of $(H_2O)_2$). If we closely examine the two formamide−water complexes, one observes, in this case, that the hydrogen bond length associated with the proton-donor character is shorter in the keto form (1.894 Å) than in the enol form (1.956 Å). Second, in each complex, one hydrogen bond connects two different atoms (O and N) whereas in water clusters hydrogen bonds are between atoms of the same type. Thus, it would be necessary to compare

SCHEME 1

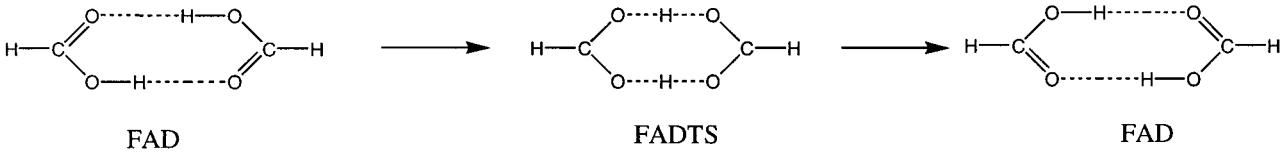

TABLE 4: O(1s), N(1s), and C(1s) CEBEs (eV) for Formamide, Formamidic Acid, Water, and the Keto and Enol Forms of the Formamide−Water Complexes[a]

				formamide−water		
	formamide	formamidic acid	water	keto	enol	binding energy shift enol/keto
NH_2COH	537.64	540.17		537.79	539.64	+1.85
NH_2COH	294.11	293.91		294.15	293.86	−0.29
NH_2COH	406.70	404.94		406.46	404.98	−1.48
H_2O			539.95	538.89	539.16	+0.27

[a] The binding energy shifts between these two forms are also reported.

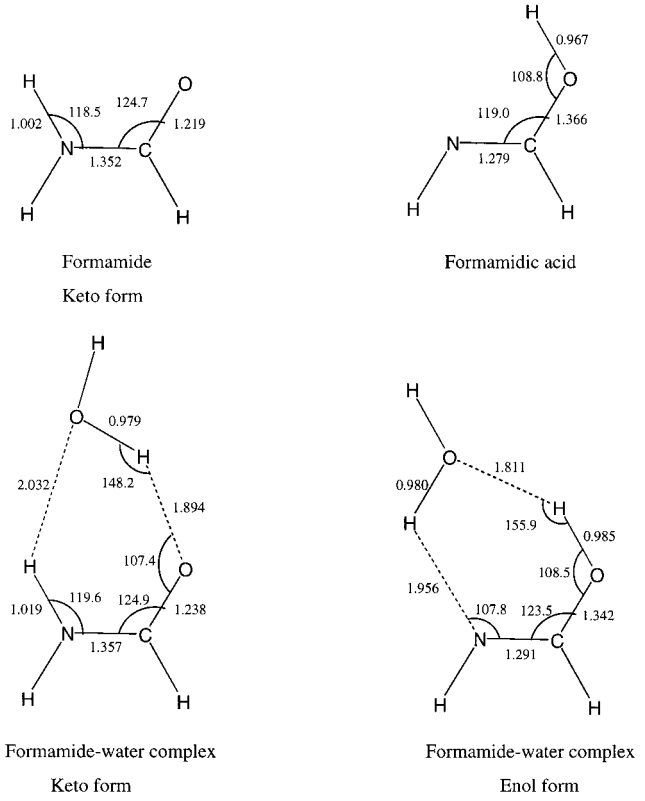

Figure 6. Geometries of the two forms of the formamide molecule (formamide and formamidic acid) and the formamide−water complex (keto and enol forms). Distances are given in angstroms and angles in degrees.

our results with other XPS spectra of molecules involving H-bonds between heteroatoms.

4. Conclusion

In this study, we have computed core−electron binding energies (CEBEs) of atoms for various clusters or complexes having strong hydrogen bonds. This was done using the recently developed ΔE_{KS} method, based on density functional theory (DFT).

Our first result is that this method correctly reproduces available experimental data featuring the dependence of O(1s) CEBEs as a function of cluster size in gas phase $(H_2O)_n$ water clusters. We obtain a shift of up to 0.93 eV ($n = 6$) with respect to the isolated water molecule, which is in fairly good agreement with experimental findings (exp: 1.1 eV), suggesting that most of the hydrogen bonding effect occurs for very small clusters.

Our present calculations quantitatively approach the experimental shifts, while our clusters are probably too small for true collective polarization screening to be taken into account. Our conclusion is thus that the interpretation of the shifts is different from the one used in the case of rare gas clusters.

We observe that the decrease of the binding energies is linearly correlated to structural properties of the hydrogen bond network, and in particular to O...O and O...H intermolecular distances. Our present interpretation of the O(1s) CEBE shift is thus that the formation of the hydrogen bond network goes with strong geometrical rearrangements, with which CEBE shifts are correlated.

Should this interpretation be correct, one would find a fairly useful way of estimating typical hydrogen bond network characteristics using XPS. More work is in progress along these lines.

References and Notes

(1) Hüfner, S. *Photoelectron Spectroscopy*; Cardona, M., Fulde, P., von Klitzing, K., Queisser, H.-J., Eds.; Springer-Verlag Springer Series in Solid-State Physics 82; Springer: Berlin, Heidelberg, 1995; p 31.

(2) Hagström, S.; Nordling, C.; Siegbahn, K. *Z. Phys.* **1964**, *178*, 439.

(3) Siegbahn, K. *ESCA: Atomic, Molecular and Solid-State Structure studied by means of Electron Spectroscopy*; Almqvist and Wiksells AB: Uppsala, 1967.

(4) Siegbahn, K. *ESCA applied to Free Molecules*; North-Holland Publishing Co.: Amsterdam, 1969.

(5) Jolly, W. L. *Electron Spectroscopy*: *Theory, Techniques and Applications*; Brundle, C. R., Baker, A. D., Eds.; Academic Press: London, New York, San Francisco, 1977; Vol. 1, p 133.

(6) See for example: Fadley, C. S. *Electron Spectroscopy*: *Theory, Techniques and Applications*; Brundle, C. R., Baker, A. D., Eds.; Academic Press: London, New York, San Francisco, 1977; Vol. 2, p 75.

(7) Gelius, U. *Phys. Script.* **1974**, *9*, 133.

(8) Naves de Brito, A.; Svensson, S.; Agren, H.; Delhalle, J. *J. Electron Spectrosc. Relat. Phenom.* **1993**, *63*, 239 and references therein.

(9) Chong, D. P. *Chem. Phys. Lett.* **1995**, *232*, 486.

(10) Cavigliasso, G.; Chong, D. P. *J. Chem. Phys.* **1999**, *111*, 9485.

(11) Slater, J. C. *Adv. Quantum Chem.* **1972**, *6*, 1.

(12) Williams, A. R.; de Groot, R. A.; Sommers, C. B. *J. Chem. Phys.* **1975**, *63*, 628.

(13) Bureau, C.; Chong, D. P.; Lécayon, G.; Delhalle, J. *J. Electron Spectrosc. Relat. Phenom.* **1997**, *83*, 227.

(14) (a) Chong, D. P. *Can. J. Chem.* **1996**, *74*, 1005. (b) Chong, D. P.; Hu, C. H.; Duffy, P. *Chem. Phys. Lett.* **1996**, *249*, 491. (c) Pulfer, M.; Hu, C.-H.; Chong, D. P. *Chem. Phys.* **1997**, *216*, 91. (d) Bureau, C.; Chong, D. P. *Chem. Phys. Lett.* **1997**, *264*, 186. (e) Kranias, S.; Bureau, C.; Chong, D. P.; Brenner, V.; George, I.; Viel, P.; Lecayon, G. *J. Phys. Chem. B* **1997**, *101*, 10254. (f) Hu, C.-H.; Chong, D. P. *Chem. Phys.* **1997**, *216*, 99. (g) Chong, D. P.; Hu, C.-H. *J. Chem. Phys.* **1998**, *108*, 8950. (h) Cavigliasso, G.; Chong, D. P. *Can. J. Chem.* **1999**, *77*, 24.

(15) (a) Chong, D. P. *Chin. J. Phys.* **2000**, *38*, 57 (b) Aplincourt, P.; Chong, D. P.; Bureau, C. Manuscript in preparation.
(16) Kranias, S.; Bureau, C.; Chong, D. P.; Brenner, V.; George, I.; Viel, P.; Suski, J.; Lécayon, G. *J. Phys. Chem. B* **1997**, *101*, 10254.
(17) Chong, D. P.; Bureau, C. *J. Electron Spectrosc. Relat. Phenom.* **2000**, *106*, 1.
(18) Fliszàr, S. *Charge Distributions and Chemical Effects*; Springer-Verlag: New York, 1983; Chapter 4.
(19) Deleuze, M. S.; Leigh, D. A.; Zerbetto, F. *J. Am. Chem. Soc.* **1999**, *121*, 2364 and references therein.
(20) Björneholm, O.; Federmann, F.; Kakar, S.; Möller, T. *J. Chem. Phys.* **1999**, *111*, 546.
(21) (a) St-Amant, A.; Salahub, D. R. *Chem. Phys. Lett.* **1990**, *169*, 387. (b) St Amant, A. *Ph.D. Thesis*, Université de Montréal, 1991.
(22) (a) Duffy, P.; Chong, D. P.; Dupuis, M. *J. Chem. Phys.* **1995**, *102*, 3312. (b) Chong, D. P. *Chin. J. Phys.* **1992**, *30*, 115.
(23) (a) Dunning, T. H., Jr. *J. Chem. Phys.* **1989**, *90*, 1007. (b) Kendall, R. A.; Dunning, T. H., Jr.; Harrison, R. J. *J. Chem. Phys.* **1992**, *96*, 6796. (c) Feller and the ECCE Team; the EMSL project, Pacific Northwest Laboratory, 1994.
(24) Chong, D. P. *J. Chem. Phys.* **1995**, *103*, 1842.
(25) Perdew, J. P.; Wang, Y. *Phys. Rev. B* **1986**, *33*, 8800.
(26) Perdew, J. P.; Wang, Y. *Phys. Rev. B* **1992**, *45*, 13244.
(27) Xantheas, S. S. Private communication, 1999.
(28) Xantheas, S. S. *J. Phys. Chem.* **1995**, *102*, 4505.
(29) (a) Hellwege, K.-L. *Landolt-Börnstein Numerical Data and Functional Relationships in Science and Technology*; Springer: Berlin, 1976; New Series, Group II, Vol. 7. (b) Madelung, O. *Landolt-Börnstein Numerical Data and Functional Relationships in Science and Technology*; Springer: Berlin, 1987; New Series, Group II, Vol. 15. (c) Madelung, O.; *Landolt-Börnstein Numerical Data and Functional Relationships in Science and Technology*; Springer: Berlin, 1992; New Series, Group II, Vol. 21.
(30) Frisch, M. J.; Trucks, G. W.; Schlegel, H. B.; Scuseria, G. E.; Robb, M. A.; Cheeseman, J. R.; Zakrzewski, V. G.; Montgomery, J. A.; Stratmann, R. E.; Burant, J. C.; Dapprich, S.; Millam, J. M.; Daniels, A. D.; Kudin, K. N.; Strain, M. C.; Farkas, O.; Tomasi, J.; Barone, V.; Cossi, M.; Cammi, R.; Mennucci, B.; Pomelli, C.; Adamo, C.; Clifford, S.; Ochterski, J.; Petersson, G. A.; Ayala, P. Y.; Cui, Q.; Morokuma, K.; Malick, D. K.; Rabuck, A. D.; Raghavachari, K.; Foresman, J. B.; Cioslowski, J.; Ortiz, J. V.; Stefanov, B. B.; Liu, G.; Liashenko, A.; Piskorz, P.; Komaromi, I.; Gomperts, R.; Martin, R. L.; Fox, D. J.; Keith, T.; Al-Laham, M. A.; Peng, C. Y.; Nanayakkara, A.; Gonzalez, C.; Challacombe, M.; Gill, P. M. W.; Johnson, B. G.; Chen, W.; Wong, M. W.; Andres, J. L.; Head-Gordon, M.; Replogle, E. S.; Pople, J. A. *Gaussian 98*, revision A.5; Gaussian, Inc.: Pittsburgh, PA 1998.
(31) Kryachko, E. S. *Chem. Phys. Lett.* **1999**, *314*, 353.
(32) Björneholm, O.; Federmann, F.; Fössing, F.; Möller, T. *Phys. Rev. Lett.* **1995**, *74*, 3017.
(33) Björneholm, O.; Fössing, F.; Federmann, F.; Möller, T.; Stampfli, P. *J. Chem. Phys.* **1996**, *104*, 1846.
(34) Buckingham, A. D.; Fowler, P. W. *Can. J. Chem.* **1985**, *63*, 2018.
(35) Almenningen, A.; Bastiansen, O.; Motzfeldt, T. *Acta Chem. Scand.* **1969**, *23*, 2848; **1970**, *24*, 747.
(36) Yokoyama, I.; Miwa, Y.; Machida, K. *J. Phys. Chem.* **1991**, *95*, 9740.
(37) Yokoyama, I.; Miwa, Y.; Machida, K. *J. Am. Chem. Soc.* **1991**, *113*, 6458.
(38) Ito, F.; Nakanaga, T. *Chem. Phys. Lett.* **2000**, *318*, 571.
(39) Chojnacki, H.; Andzelm, J.; Nguyen, D. T.; Sokalski, W. A. *Comput. Chem.* **1995**, *19*, 181.
(40) Qian, W.; Krimm, S. *J. Phys. Chem.* **1996**, *100*, 14602.
(41) Qian, W.; Krimm, S. *J. Phys. Chem. A* **1998**, *102*, 659.
(42) Jursic, B. S. *J. Mol. Struc.* (*THEOCHEM*) **1997**, *417*, 89.
(43) Svensson, P.; Bergman, N.-A.; Ahlberg, P. *J. Chem. Soc., Chem. Commun.* **1990**, *12*, 862.
(44) Shida, N.; Barbara, P. F.; Almlöf, J. *J. Chem. Phys.* **1991**, *94*, 3633 and references therein.
(45) Kim, Y. *J. Am. Chem. Soc.* **1996**, *118*, 1522.
(46) Miura, S.; Tuckerman, M. E.; Klein, M. L. *J. Chem. Phys.* **1998**, *109*, 5290.
(47) Kohanoff, J.; Koval, S.; Estrin, D. A.; Laria, D.; Abashkin, Y. *J. Chem. Phys.* **2000**, *112*, 9498.
(48) Lim, J.-H.; Lee, E. K.; Kim, Y. *J. Phys. Chem. A* **1997**, *101*, 2233.
(49) Jolly, W. L.; Bomben, K. D.; Eyermann, C. J. *At. Data Nucl. Data Tables* **1984**, *31*, 433.
(50) Chalmet, S.; Ruiz-López, M.-F. *J. Chem. Phys.* **1999**, *111*, 1117.
(51) Rablen, P. R.; Lockman, J. W.; Jorgensen, W. L. *J. Phys. Chem. A* **1998**, *102*, 3782.
(52) Cristinziano, P.; Lelj, F.; Amodeo, P.; Barone, G.; Barone, V. *J. Chem. Soc., Faraday Trans.* **1989**, *85*, 621.
(53) Sobolewski, A. L. *J. Photochem. Photobiol. A* **1995**, *89*, 89.
(54) Wang, X.-C.; Nichols, J.; Feyereisen, M.; Gutowski, M.; Boatz, J.; Haymet, A. D. J.; Simons, J. *J. Phys. Chem.* **1991**, *95*, 10419.